

## Enhancing efficiency in capacitive power transfer: exploring gap distance and load robustness

Yusmarnita Yusop, Yan Qi Cheok, Shakir Saat, Huzaimah Husin

Faculty of Electronics and Computer Engineering and Technology (FTKEK), Universiti Teknikal Malaysia Melaka, Melaka, Malaysia

### Article Info

#### Article history:

Received Aug 30, 2023

Revised Mar 19, 2024

Accepted Apr 2, 2024

#### Keywords:

Capacitive power transfer

Class-E LCCL inverter

LC matching circuit

Wireless power transfer

Zero-voltage switching

### ABSTRACT

In this paper, the capacitive power transfer (CPT) technology is used as an alternative to inductive power transfer (IPT). CPT relies on electric fields that are not sensitive to the presence of any metals, utilizes metal electrodes for power transfer, and is less bulky compared to IPT. The proposed CPT system utilizes a Class-E resonant inverter with a double-sided inductor-capacitor (LC) matching circuit which operates at an optimum load,  $R_L = 50 \Omega$  with a duty cycle,  $D=0.5$  to gain an output power,  $P_o = 8.02$  W and efficiency,  $\eta=84.6\%$ . The proposed CPT system enhances the system's efficiency as compared to the past research while preserving the zero-voltage switching (ZVS) condition within a wider load range from  $50 \Omega$  to  $1,316 \Omega$ . This paper also shows that the proposed CPT system is less sensitive to load and coupling variations. Finally, the rate of power dissipated at varied load resistances,  $\frac{dP_o}{dR_L}$  has been derived successfully to determine the sensitivity level of the proposed CPT systems toward load variations. These equations are then validated by plotting the efficiency graphs based on load and coupling variations.

This is an open access article under the [CC BY-SA](https://creativecommons.org/licenses/by-sa/4.0/) license.



### Corresponding Author:

Yusmarnita Yusop

Faculty of Electronics and Computer Engineering and Technology (FTKEK), Universiti Teknikal Malaysia Melaka

Jalan Hang Tuah Jaya, 76100 Durian Tunggal, Melaka, Malaysia

Email: yusmarnita@utem.edu.my

## 1. INTRODUCTION

In recent years, there have been significant advancements in wireless power transfer technology, and capacitive power transfer (CPT) has emerged as a promising alternative to inductive power transfer (IPT). CPT enables wireless transmission of energy over short distances between a power source and a device without the need for physical connectors. This technology stands out as it relies on electric fields that are not sensitive to the presence of any metals [1], [2]. Additionally, the utilization of cost-effective metal electrodes distinguishes CPT from IPT, which requires high-cost Litz wire coils [3]. Furthermore, the reduced bulkiness of CPT further positions it as a compelling alternative to IPT, which utilizes Litz wire coils [4], contributing to a more cumbersome design.

Figure 1 shows the block diagram of a CPT system, comprising a transmitter unit, an energy medium transfer, and a receiver unit. Operating on the principle of electrostatic coupling, CPT involves four capacitive couplers, two located at the transmitter and the other two at the receiver. In the transmitter unit, the high-frequency inverter converts the direct current (DC) power supply to high-frequency alternating current (AC) voltage and supplies it to the capacitive plates at the primary side (transmitting plates). Therefore, an electric field is established to carry the energy across the medium to the capacitive plates at the secondary side (receiving plate). Then, the rectifier captures the energy from the electric field and converts it to

electrical power that could be used by the load. For both transmitter and receiver units, compensation circuits are required to cancel the reactive power, achieving the zero-voltage switching (ZVS) for the CPT [5], [6].

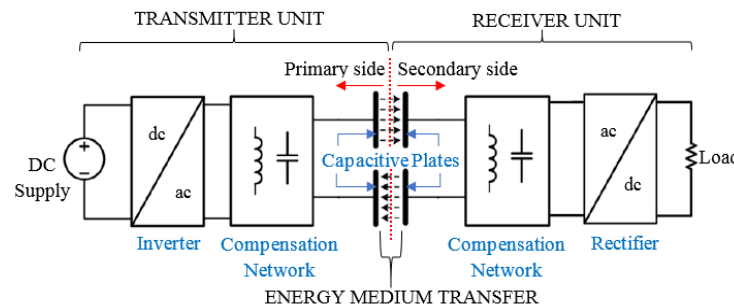


Figure 1. Block diagram of capacitive power transfer (CPT) [7]

Designing a CPT system involves several design issues and challenges to ensure efficient and safe power transfer over distances. These design issues encompass the intricate management of electric fields and ensuring safety, achieving optimal energy transfer efficiency, and accommodating variable loads and gap distances to enhance performance. Notably, CPT is adopted for low or medium power levels and small air gaps [4]. According to recent studies, CPT technology is being employed in low-power charging applications with output power,  $P_o \leq 20 W$  and small air gap distance,  $d \leq 2 mm$  in drone [8], [9], variable message sign [10], rotary device [11], [12] and dynamic load [13]. By considering the electric field management and safety issue, a large air gap and high power would cause the electric field emission to exceed the established threshold, as outlined by the IEEE standard of 614 V/m [14]. Therefore, any design of a CPT system should not exceed this limit; otherwise, it might not be safe for human contact [15]. Besides, to protect humans against adverse health effects when exposed to very high radio frequency, National Council on Radiation Protection and Measurements (NCRP), Institute of Electrical and Electronics Engineers (IEEE), and International Commission on Non-Ionizing Radiation Protection (ICNIRP) determined a threshold level of specific absorption rate (SAR) of about 0.4 W/kg [14]. Therefore, a suitable operating frequency for the CPT system within the permitted SAR is important to allow maximum power transfer.

Another design issue to be aware of when designing a CPT system is energy transfer efficiency. The CPT system may suffer efficiency losses from the power converter, coupling plates, and rectifier due to switching losses [16], coupling losses [17], and parasitic resistance losses [18]. Therefore, the selection of a power converter is of utmost importance in the CPT system. Recently, most researchers prefer the bridge converter [8], [9], [13], [19]–[21] and the Class-E converter [11], [12], [22]–[24]. However, the bridge converter has two drawbacks, it needs complicated drivers and its efficiency is lower than a Class-E converter. Theoretically, the Class-E topology can achieve 100% efficiency [25], [26]. Besides, it allows the CPT system to operate in ZVS conditions, thus reducing power loss. Therefore, the Class-E converter is more suitable for realizing a CPT system. The power loss from coupling plates may be due to the misalignment. Thus, the capacitive coupler designs such as four-plate [8], [9], [12], [13], [20], [21], [24] and multiple plates [7], [27] are applied by the researchers to reduce the sensitivity of the CPT system toward the variation in alignments. This design approach helps to maintain a more stable and efficient power transfer of the CPT system [28], [6]. Additionally, the full-wave rectifier [20] including the use of Schottky diodes is considered in designing a CPT system to minimize power dissipation [29] and enhance performance. Schottky diodes are suggested due to their low forward voltage drop or low turn-on time, resulting in minimal power dissipation. Besides, these diodes possess high switching speeds and can operate at very high frequencies.

Impedance matching circuits, such as  $\pi 2a$  developed by Ayachit [10] and the  $\pi 1a$  circuit developed by Meor [22] are commonly integrated into the CPT system. These circuits help to match or transform the input and output impedance, thereby minimizing signal reflections and improving power transfer. However, these circuits are only effective for a fixed load resistance value. Any change in load resistance will result in decreased system efficiency and increased power dissipation. This is because CPT is sensitive to variations in load and coupling [21], [30]. Addressing impedance matching challenges, this paper introduces a double-sided inductor-capacitor (LC) matching circuit. This circuit includes one pair of LC matching circuits at both the transmitter and receiver sides, providing greater flexibility in circuit tuning. Furthermore, the presence of multiple reactive components on both sides enables the adjustment of impedance over a wider range to accommodate different loads, while also reducing sensitivity to load and coupling variations. Besides, the

size of the capacitive coupler is reduced as more reactive components are added, resulting in a decrease in capacitance to 120.85 pF. The proposed matching circuits extend the load range from the optimum load, 50 Ω up to 1,316 Ω, surpassing the capabilities of the π1b matching circuit applied by with same voltage supply [31].

Finally, incorporating the design issues and solutions discussed above, this paper proposed a CPT system that utilizes a Class-E resonant inverter with a double-sided LC matching circuit (Class-E LCCL circuit). Operating under specific conditions, this system achieves the ZVS condition with a remarkable 10W output power, an efficiency above 80%, and a wider load range from 50 Ω to 1,316 Ω. To prove the ZVS condition, the waveforms of drain-to-source voltage,  $V_{ds}$  and current,  $I_{ds}$  are provided. Notably, this paper demonstrates the ability of LC matching to withstand changes in load and coupling variations when compared to π1b matching, as evidenced by the efficiency graphs and the rate of power,  $\left(\frac{dP_o}{dR_L}\right)$  presented. ZVS condition was achieved Nevertheless, the following sections explore in-depth analysis, mathematical calculations, and experimental confirmations that substantiate the proposed CPT system. Additionally, a full-wave rectifier is applied in the proposed CPT system due to its filtering effect when used in conjunction with the capacitor filter, but its power dissipation is still considerable.

**2. METHOD**

**2.1. Class-E with double-sided LC compensation circuit (Class-E LCCL circuit)**

The design of the CPT system began with the construction of the inverter part which was a Class-E LCCL circuit without a rectifier as shown in Figure 2. It clearly shows the position of two LC compensation networks, one located at the transmitter and another located at the receiver to compensate for the losses from both sides. In this case, the capacitor  $C_3$  which acts as capacitive coupler. The temporary resistor,  $R_o$  is the imaginary resistor that is used to match the reactance of the capacitor  $C_3$  at transmitter side and also the impedance of the receiver side.

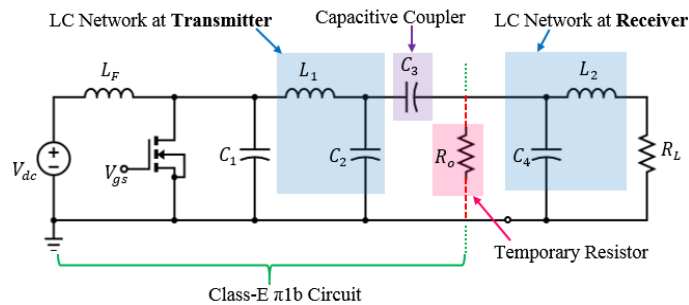


Figure 2. Class-E double-sided LC impedance matching circuit (Class-E LCCL circuit)

The following assumptions are made when designing the Class-E LCCL circuits: i) The MOSFET and its internal diode form an ideal switch with zero on-resistance, infinite off-resistance, and zero switching times; ii) The choke inductance  $L_F$  is high so that the AC ripple on the DC supply current  $I_{dc}$  can be neglected; iii) The loaded quality factor  $Q$  of the  $L-C_2-R_L$  a series-resonant circuit is high enough so that the output current  $i_o$  through the resonant circuit is sinusoidal; iv) All components are ideal, and the switch voltage satisfies ZVS conditions; and v) The circuit operation is within the interval  $0 < \omega t \leq 2\pi$  and the duty cycle is 50%.

Figure 3 shows the simplification of Class-E LCCL circuits where the Class-E LCCL circuit in Figure 3(a) can be transformed into a Class-E π1b circuit in Figure 3(b) and finally into a Class-E resonant circuit in Figure 3(c) to ease the derivation. All the related equations of the circuit parameters can be modified from the equations of Class-E π1b circuit and Class-E resonant inverter as shown in the previous works of Yusop cited as [31] and [32], respectively. The equations for the proposed CPT system (Class-E LCCL circuits) are shown.

The maximum switch voltage,  $V_{ds}(peak)$  is expressed as (1):

$$\frac{v_{ds}(\omega t)}{V_{dc}} = \begin{cases} 0 & , \text{for } 0 < \omega t \leq \pi \\ \pi \left[ \omega t - \frac{3\pi}{2} - \frac{\pi}{2 \cos \phi} \cos(\omega t + \phi) \right] \approx 3.558 & , \text{for } \pi < \omega t \leq 2\pi \end{cases} \quad (1)$$

The maximum switch current,  $I_{ds}(peak)$  is expressed as (2)

$$\frac{i_{ds}(\omega t)}{I_{dc}} = \begin{cases} 1 - \frac{\sqrt{\pi^2+4}}{2} \sin(\omega t + \varphi) \approx 2.862 & , for 0 < \omega t \leq \pi \\ 0 & , for \pi < \omega t \leq 2\pi \end{cases} \quad (2)$$

The series resistance,  $R_{To}$  can be expressed as:

$$R_{To} = \frac{8V_{dc}^2}{(\pi^2+4)P_o} \quad (3)$$

The choke inductance,  $L_f$  can be expressed as:

$$L_{F(min)} = 2 \left( \frac{\pi^2}{4} + 1 \right) \frac{R_{To}}{f} \quad (4)$$

The shunt capacitance,  $C_1$  can be expressed as:

$$C_1 = \frac{8}{\omega R_{To} \pi (\pi^2+4)} \quad (5)$$

The transmitter matching inductance,  $L_1$  can be expressed as:

$$L_1 = \frac{Q_L R_{To}}{\omega} \quad (6)$$

The transmitter matching capacitance,  $C_2$  can be expressed as:

$$C_2 = \frac{Q_L - \frac{\pi(\pi^2-4)}{16}}{\omega R_{To}} \sqrt{\frac{R_{To} \left[ 1 + \left( Q_L - \frac{\pi(\pi^2-4)}{16} \right)^2 \right]}{R_o} - 1} \quad (7)$$

The coupling capacitance,  $C_3$  can be expressed as:

$$C_3 = \frac{2}{\omega R_{To} \left[ \left( Q_L - \frac{\pi(\pi^2-4)}{16} \right)^2 + 1 \right]} \quad (8)$$

The receiver matching inductance,  $L_2$  can be expressed as:

$$L_2 = \frac{\sqrt{R_o R_L - R_L^2}}{2\pi f} \quad (9)$$

The receiver matching capacitance,  $C_4$  can be expressed as:

$$C_4 = \frac{L_2}{R_o R_L} \quad (10)$$

By assuming  $R_o = C_3$ , therefore the resistance of the temporary resistor,  $R_o$  can be expressed as:

$$R_o = X_{C3} = \frac{1}{\omega C_3} \quad (11)$$

The sensitivity of the proposed CPT system can be measured through the rate of power dissipated when the load varies or denotes as derivative of a power with respect to load,  $\frac{dP_o}{dR_L}$ . In mathematics, the derivative of a function of a real variable measures the sensitivity of changing function value (output value) with respect to a change in its argument (input value) [33]. The  $\frac{dP_o}{dR_L}$  value should be as small as possible because the smaller the value of  $\frac{dP_o}{dR_L}$ , less power loss during load variations, less sensitive the circuit towards

the load variations. The  $\frac{dP_o}{dR_L}$  can be reduced by adding multiple reactive components such as inductor and capacitor to compensate the switching loss in switch while maintain its ZVS [34].

The  $\frac{dP_o}{dR_L}$  for Class-E  $\pi 1b$  Circuit:

$$\frac{dP_o}{dR_L} = \frac{8V_{dc}^2}{(\pi^2+4)} \left[ W^2 C_2^2 - \frac{(C_2+C_3)^2}{C_3^2 R_L^2} \right] \tag{12}$$

The  $\frac{dP_o}{dR_L}$  for Class-E LCCL Circuit:

$$\frac{dP_o}{dR_L} = \frac{8V_{dc}^2}{(\pi^2+4)} \left\{ \frac{\omega^2 C_2^2 (1-\omega^2 C_4 L_2)^2 - \omega^4 C_2^2 C_4^2 R_L^2}{[(1-\omega^2 C_4 L_2)^2 + \omega^2 C_4^2 R_L^2]^2} + \left( \frac{C_2+C_3}{C_3} \right)^2 \left[ \omega^2 C_4^2 - \frac{(1-\omega^2 C_4 L_2)^2}{R_L^2} \right] \right\} \tag{13}$$

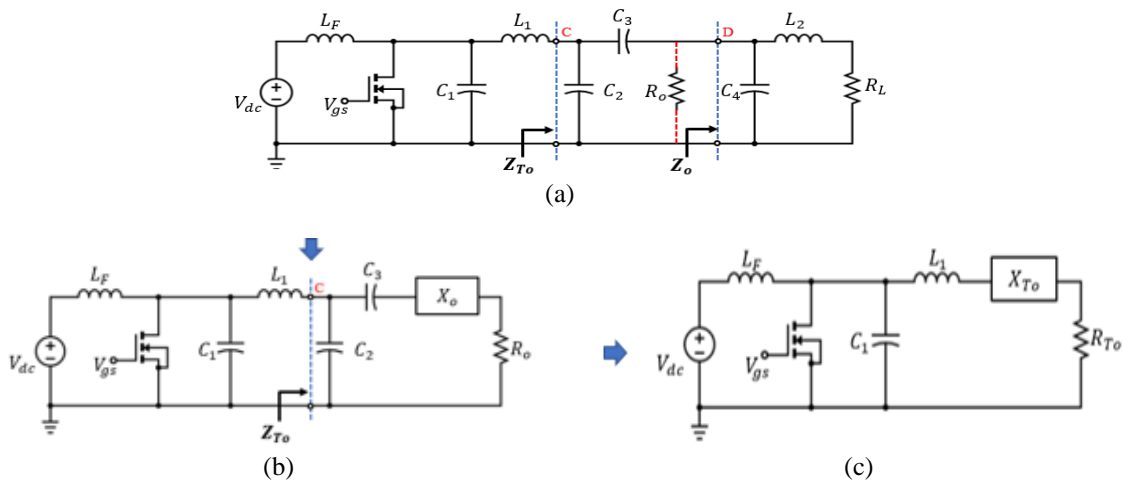


Figure 3. Simplification of Class-E LCCL circuits with (a) Class-E LCCL circuit, (b) Class-E  $\pi 1b$  circuit and (c) Class-E resonant inverter

**2.2. Full-wave rectifier**

The Class-E LCCL circuit combines with a full-wave rectifier as shown in Figure 4 to rectify the output from AC to pulsating DC. Then, the capacitor filter rectifies the pulsating DC to a steady DC which is more suitable for a load. The capacitance of the capacitor filter,  $C_f$  is calculated by assuming the peak-to-peak ripple voltage,  $V_{ripple}$  to be less than 10% of the output voltage,  $V_{RL}$ .

$$C_f = \frac{I_{RL(rms)}}{f V_{ripple}} = \frac{I_{RL(rms)}}{f \times 0.1 V_{RL}} \tag{14}$$

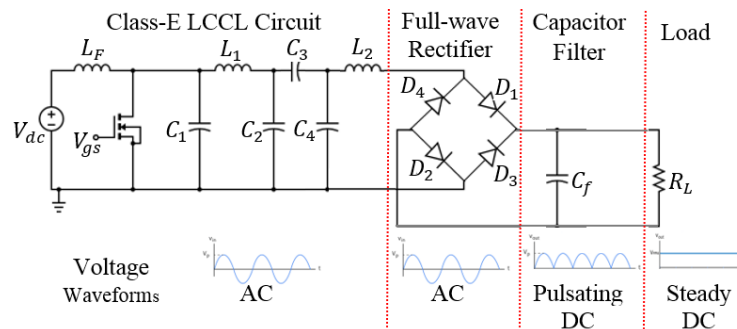


Figure 4. Class-E LCCL circuit with full-wave rectifier

### 2.3. Capacitive coupler

The capacitor  $C_3$  in Class-E LCCL circuit was modified to a bipolar structure of capacitive coupler as shown in Figure 5 to realize a CPT system. The bipolar structure was selected as it is more effective for power transfer [6], [28], [35], [36]. Moreover, the capacitor  $C_3$  in Class-E LCCL circuit was selected to be modified into coupling plates because it is in series with the load and can separate the circuit into the primary side and secondary side. Both sides are isolated from each other to allow a certain degree of flexibility and movement.

Firstly, the capacitor  $C_3$  was separated into two capacitors, namely capacitors  $C_{31}$  and  $C_{32}$  which connected in series. By assuming  $C_{31} = C_{32}$ , the capacitance of the capacitor  $C_{31}$  and  $C_{32}$  became twice of capacitor  $C_3$  as shown in (14). The capacitor  $C_{31}$  and  $C_{32}$  were then replaced with two pairs of circular copper plates, named as  $P_1, P_2, P_3$ , and  $P_4$ . The area of the copper plates was calculated by the equation of total equivalent capacitance shown in (15).

$$C_3 = \frac{C_{31} \times C_{32}}{C_{31} + C_{32}} = \frac{(C_{31})^2}{2C_{31}} = \frac{1}{2} C_{31} \quad \text{or} \quad C_{31} = C_{32} = 2C_3 \quad (15)$$

$$C_3 = \frac{\epsilon_0 \epsilon_r A}{d} \quad (16)$$

where  $\epsilon_0$  = permittivity of vacuum =  $8.854 \times 10^{-12}$  F/m;  $\epsilon_r$  = relative permittivity of the dielectric constant (air) = 1.0006;  $A$  = area of the capacitive plates =  $r^2$ ; and  $d$  = distance between the capacitive coupler = 1 mm.

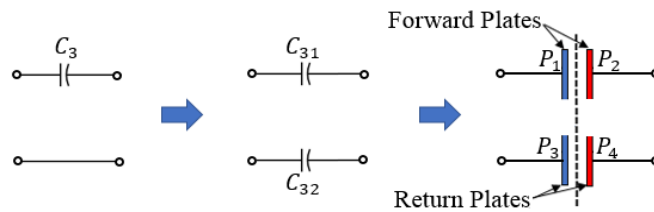


Figure 1. Transformation of a single capacitor to coupling plates

### 2.4. Efficiency

The input power, output power, and efficiency of the CPT system are calculated to determine the output performance of the proposed CPT system. The input power,  $P_{i(dc)}$  of the circuit is expressed as (17):

$$P_{i(dc)} = V_{dc} \times I_{dc} = \pi \omega C_1 V_{dc}^2 \quad (17)$$

The output power,  $P_{o(ac)}$  of the Class-E LCCL circuit is expressed as (18):

$$P_{o(ac)} = \frac{8 V_{dc}^2}{(\pi^2 + 4) R_L} \quad (18)$$

The efficiency of the of the Class-E LCCL circuit is expressed as (19):

$$\eta = \frac{P_{o(ac)}}{P_{i(dc)}} \times 100\% \quad (19)$$

## 3. RESULTS AND DISCUSSION

### 3.1. Capacitive coupler design

Figures 6(a) and 6(b) show the front and side views for the circular capacitive coupling plates used in the CPT system. The coupling plates were made from single-sided FR4 printed circuit board (PCB) copper plate, which was easier to find and cheaper. The values of the capacitor  $C_3$  in Figure 2 was calculated from (8) which is equal to 120.85 pF. Then, it was modified to two pairs of round coupling plates with  $C_{31} = C_{32} = 241.70$  pF each as mentioned in (15). The radius of the coupling plates,  $r = 66$  mm can be obtained from (16) as area of circular plate,  $A = \pi r^2$ . The capacitances of both coupling plates that connected in series were examined by using the Keysight 4285A Precision LCR meter which can be viewed in Figure 6(c).

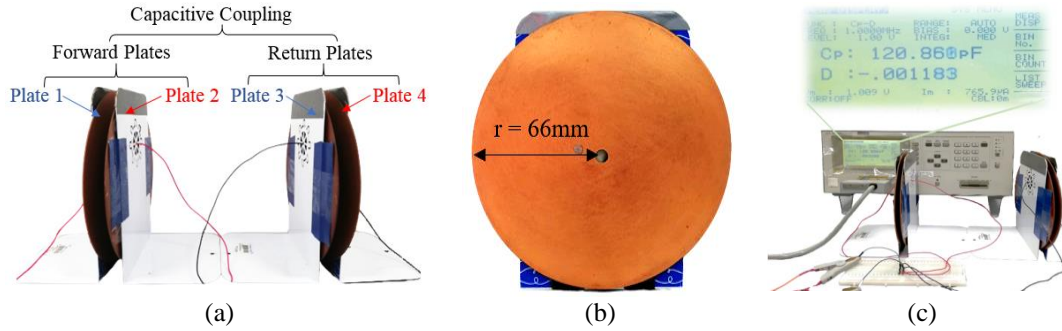


Figure 6. Capacitive coupling plates (a) in front view and (b) in side view and (c) capacitance

3.2. CPT system design

Table 1 shows the design specifications and circuit parameters of the proposed CPT system calculated from (3)-(11). Calculation was made by using (17)-(19) to predict the output performance of the circuit. Then, the output performances were verified through simulation via Simulink of MATLAB and validated through experiments in terms of ZVS, output power, and efficiency. The results are arranged in Table 2.

Table 1. Design specifications and circuit parameters of proposed CPT system

Design specifications			Circuit parameter		
Parameter	Unit	Design value	Parameter	Unit	Design value
$P_o$	W	10	$L_F$	$\mu$ H	500
$f$	MHz	1	$C_1$	pF	879.52
$V_{dc}$	V	24	$L_1$	$\mu$ H	52.88
$D$		0.50	$C_2$	pF	474.14
$Q_L$		10	$C_3$	pF	120.85
$R_L$	$\Omega$	50	$C_4$	pF	608.55
$R_o$	$\Omega$	1316	$L_2$	$\mu$ H	40.04

Table 2. Output performance of proposed CPT system

Parameter	Unit	Calculation	Simulation	Experiment
Input Voltage, $V_{dc}$	V	24	24	23.70
Input Current, $I_{dc}$	A	0.42	0.46	0.40
Input Power, $P_{in}$	W	10	11.04	9.48
Output Voltage, $V_{RL(rms)}$	V	22.36	22.10	21.10
Input Current, $I_{RL(rms)}$	A	0.45	0.44	0.38
Output Power, $P_{out}$	W	10.0	9.72	8.02
Efficiency, $\eta$	%	100	88.04	84.60
Maximum Switch Voltage, $V_{ds}$	V	86.39	86.33	86.30
Voltage across capacitor $C_2$ , $V_{C2}$	V	229.43	230.40	211
Voltage across capacitor $C_3$ , $V_{C3}$	V	162.23	161.35	157
Current across capacitor $C_3$ , $I_{C3}$	A	0.12	0.12	0.12
Voltage across capacitor $C_4$ , $V_{C4}$	V	162.23	160.80	155
Voltage across inductor $L_2$ , $V_{L2}$	V	159.12	157.75	153

Figure 7 shows the simulated CPT system in Simulink of MATLAB R2015b. The simulated switch voltage  $V_{ds(max)}$  of Class-E DC-DC converter is 86.33 V. Therefore, the IRF740 power MOSFET was applied as an inverter-switching device in the prototype. As for the full-wave rectifier circuit at the receiver side, Schottky barrier rectifier diodes (1N5819) were chosen due to their extremely low forward voltage and fast switching diode which reduces the power loss on the receiver side. A Keysight Technologies DSO-X 2012A 100 MHz oscilloscope was used to generate the desired switching control signal frequency at 50% duty cycle through its WaveGen (built-in function generator). It was very convenient to fine-tune the duty cycle,  $D$ , and the switching frequency,  $f$  that was required. Finally, a prototype of 10 W output power for the proposed CPT system was built by employing discrete components and a printed PCB, as shown in Figure 8 to validate the proposed method and investigate the output performances. The experiment setup for the CPT System with both pairs of round capacitive coupling plates is shown in Figure 9.

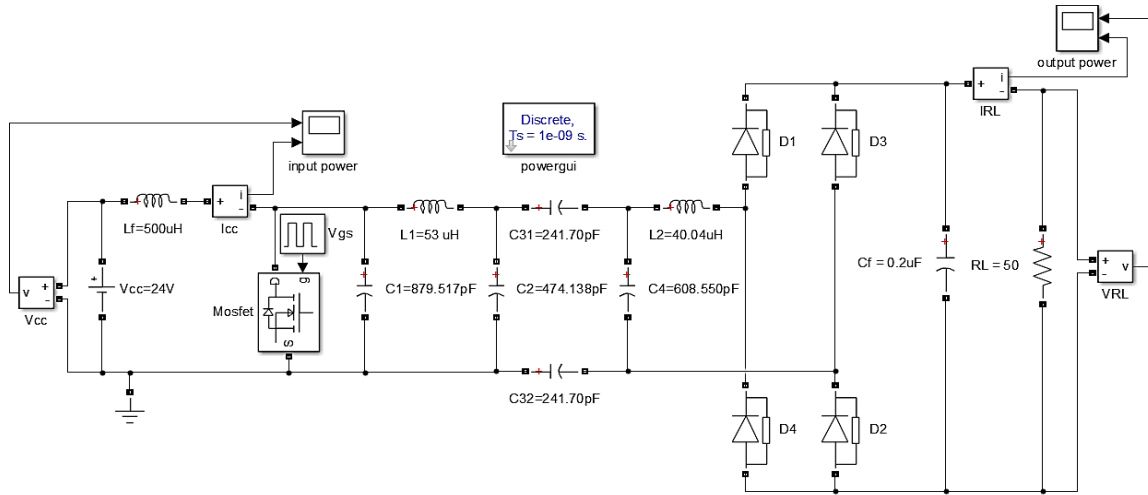


Figure 7. Simulation circuit for the proposed CPT system

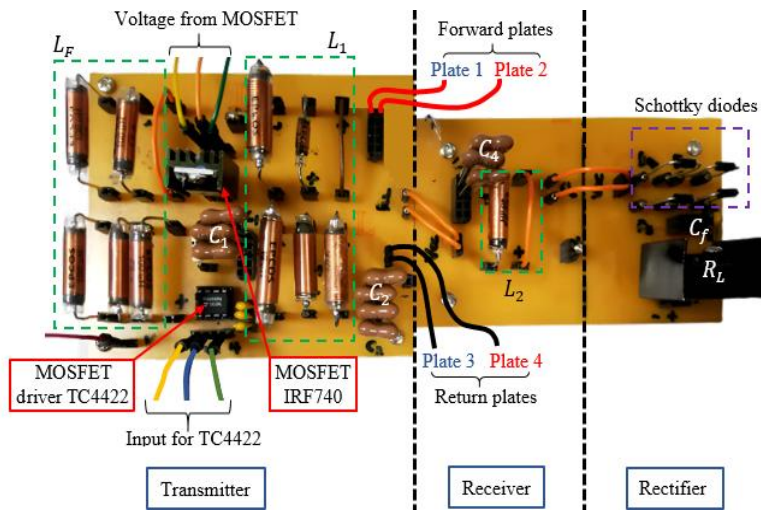


Figure 8. Circuit configuration of CPT system

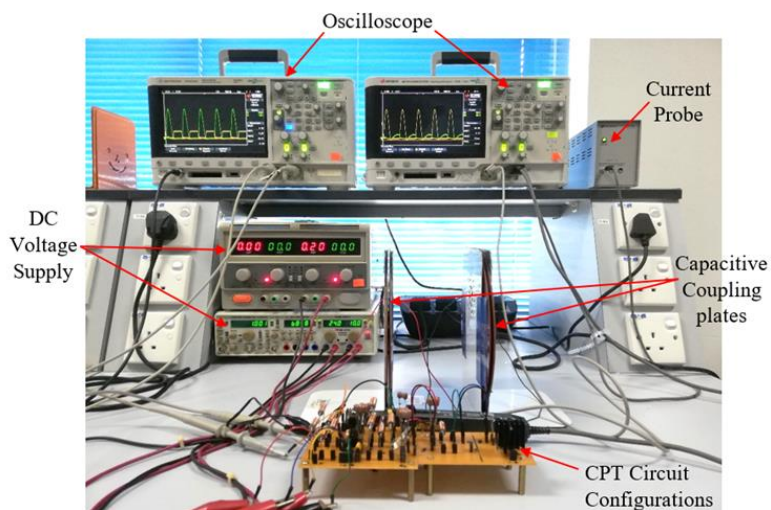


Figure 9. Experiment setup for the proposed CPT system



### 3.3. Output performance of CPT system

#### 3.3.1. ZVS condition

ZVS condition is important in the CPT system to minimize power loss and improve the efficiency of the system [37]. Therefore, the effect on switching performances of the proposed CPT system at optimum operation was investigated in Figure 10 and Figure 11, for MATLAB simulation and experiment. Figure 10 shows the switching voltage waveform of MOSFET, depicting the gate-to-source voltage,  $V_{gs}$  in Figure 10(a) and drain-to-source voltage,  $V_{ds}$  in Figure 10(b). Figure 11(a) displays the waveform of drain-to-source voltage,  $V_{ds}$  while Figure 11(b) illustrates the waveform of switch current,  $I_{ds(peak)}$ . The gate-to-source voltage,  $V_{gs}$  applied in the CPT system was 10 V for both simulation and experiment.

During MOSFET (switch) turns OFF, the maximum drain-to-source voltage,  $V_{ds(peak)}$  across switch was 85.75 V in simulation and 86.20 V in experiment. Both conditions obey the optimum condition mentioned in (1) as  $V_{ds(peak)}$  during switch turns off was almost three times greater than the input voltage,  $V_{dc}$ . The experimental  $V_{ds(peak)}$  is almost identical to the simulated  $V_{ds(peak)}$  when the switch is turned off.

If the switch voltage  $V_{ds(peak)}$  at switch turns ON is 10% to 50% of the switch voltage  $V_{ds(peak)}$  at switch turns off, a CPT system reflects a non-zero voltage switching condition [38]. During MOSFET (switch) turns ON,  $V_{ds(peak)}$  for simulation and experiment were measured at 0 V and 3.1 V, respectively. These values were equivalent to 0% and 3.6% of the  $V_{ds(peak)}$  during MOSFET turned off. Since the simulated and experimental  $V_{ds(peak)}$  were not within the range, therefore the proposed CPT system still preserve the ZVS condition and able to achieve the optimum design that yielded maximum drain efficiency.

Nevertheless, the simulated and experimental  $I_{ds(peak)}$  were 1.00 A and 1.10 A, respectively. These results were found to agree with (2), which is two times larger than the input current. In this case,  $I_{ds}$  is in phase with  $V_{gs}$ , therefore the waveform of  $V_{gs}$  could represent  $I_{ds}$  to determine the ZVS condition. Since there was no overlap between the gate-to-source voltage,  $V_{gs}$  and drain-to-source voltage,  $V_{ds}$  or switch current,  $I_{ds}$  and drain-to-source voltage,  $V_{ds}$ , ZVS condition was achieved in both simulation and experiment.

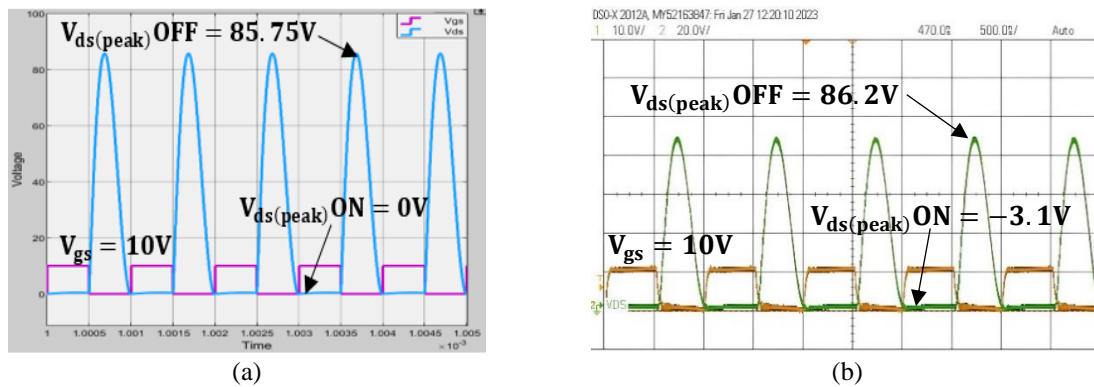


Figure 10. MOSFET switching voltages,  $V_{gs}$  and  $V_{ds}$  in (a) simulation and (b) experiment

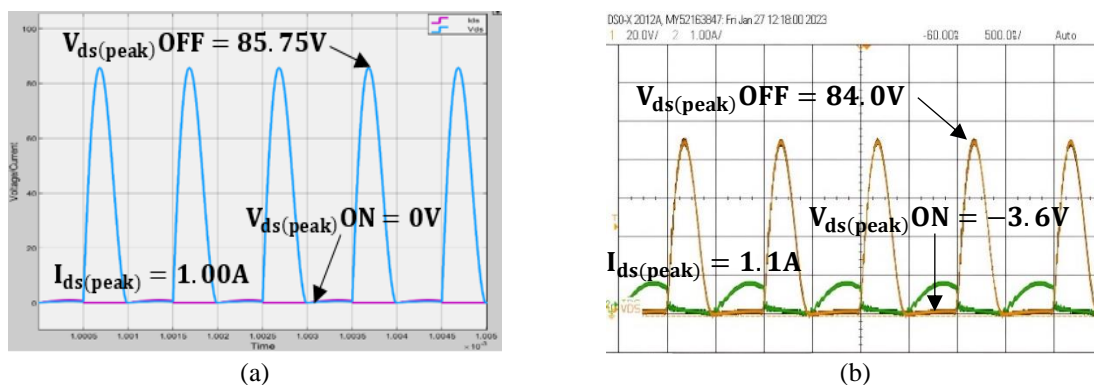


Figure 11. MOSFET switching voltage and current,  $V_{ds}$  and  $I_{ds}$  in (a) simulation and (b) experiment

### 3.3.2. Efficiency

The CPT system's efficiency was calculated using (19). By referring to Figure 12(a), the simulated input power of the CPT system was 11.04 W while from Figure 13(a), the simulated output power was 9.72 W. Therefore, the CPT system yielded an efficiency of 88.04% for simulation results. On the other hand, the experimental input and output power could be calculated from Figure 12(b) and Figure 13(b), which were 9.48 W and 8.02 W, respectively, yielding an efficiency of 84.60%. Therefore, the experimental results were 3.44% lower than the simulation result.

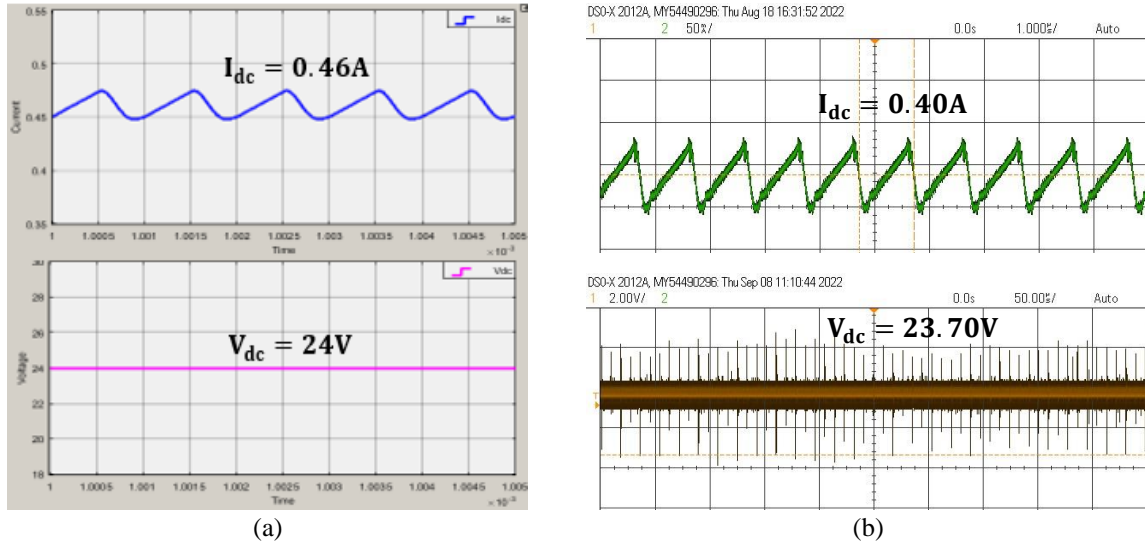


Figure 12. Waveform of input current and voltage,  $I_{dc}$  and  $V_{dc}$  in (a) simulation and (b) experiment

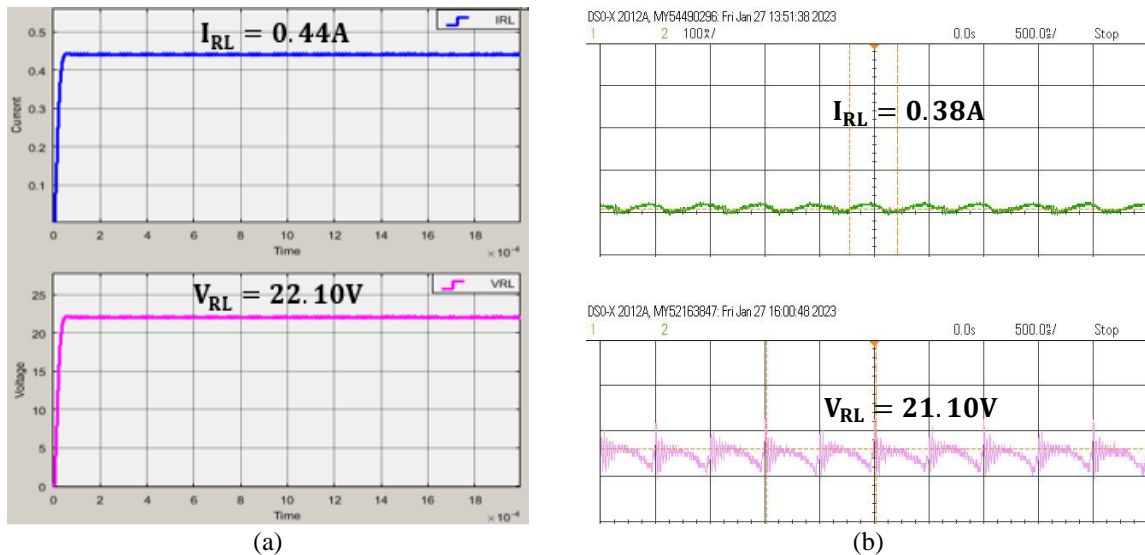


Figure 13. Output current and voltage,  $I_{RL}$  and  $V_{RL}$  in (a) simulation and (b) experiment

### 3.3.3. Load variation between Class-E LCCL circuit and Class-E $\pi 1b$ circuit

To prove the reduced sensitivity of the Class-E LCCL circuit towards the load variation in comparison to the Class-E  $\pi 1b$  circuit, two distinct methodologies were employed. The initial approach involved the calculation of the derivative of the power dissipated,  $\frac{dP_o}{dR_L}$  value at optimum load,  $R_L = 50 \Omega$ . Subsequently, the second method entailed generating an efficiency-load variation graph for comprehensive analysis.

**3.3.4.  $\frac{dP_o}{dR_L}$  analysis**

From (12) and (13), the calculated  $\frac{dP_o}{dR_L}$  value for the Class-E LCCL circuit and Class-E  $\pi$ 1b circuit were 0.0410 and 0.1997 respectively. Hence, The Class-E LCCL circuit is less sensitive to the load variation since it has smaller  $\frac{dP_o}{dR_L}$  value.

**3.3.5. Load variation graph**

Figure 14 shows the system’s efficiency for the Class-E LCCL circuit and Class-E  $\pi$ 1b circuit when varying the load resistance from 5  $\Omega$  to 2,000  $\Omega$ . The optimum load,  $R_L(opt)$  for both circuits is 50  $\Omega$  which indicates that both circuits achieved the highest efficiency at this point. From Figure 14, it was seen that the Class-E LCCL circuit was able to maintain high efficiency above 85% throughout the experiment. However, the efficiency of the Class-E  $\pi$ 1b decreases significantly when the load resistance increases. This situation proves that the Class-E LCCL circuit is less sensitive to load variation when compared to the Class-E  $\pi$ 1b circuit. Therefore, Class-E LCCL is the better choice to be implemented for the CPT system.

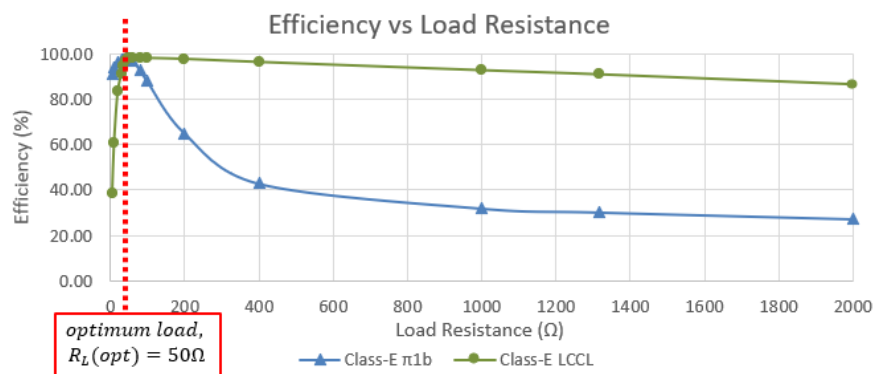


Figure 14. Efficiency vs load resistance

**3.3.6. Coupling variation between Class-E LCCL circuit and Class-E  $\pi$ 1b circuit**

Figure 15 shows the system’s efficiency for the Class-E LCCL circuit and Class-E  $\pi$ 1b circuit when varying separation distance between capacitive plates. To ease the simulation, the capacitive plates are assumed as square plates with a length of 10cm. Then, by using (16) to calculate the corresponding coupling capacitance  $C_3$ , the efficiency at varied gap distance is observed. From Figure 15, it can be clearly shown that the efficiency of the Class-E  $\pi$ 1b circuit drops significantly to nearly zero when the gap distance increases. Unlike the Class-E  $\pi$ 1b circuit, the efficiency of the Class-E LCCL circuit decreases gradually. Based on this simulation analysis on the effect of gap distance variations for both topologies, it can be concluded that the Class-E LCCL circuit efficiency appeared to be more robust because it is less sensitive to the gap distance variation when compared to Class-E  $\pi$ 1b Circuit.

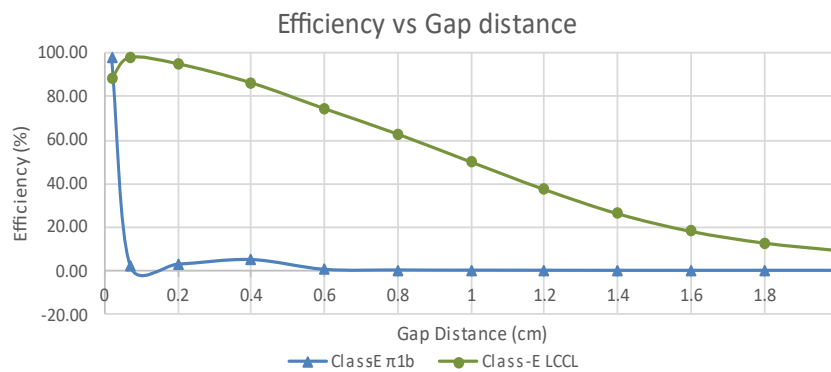


Figure 15. Graph of efficiency vs gap distance

### 3.4. Summary of the result

Table 3 shows the comparison of past research for low-power CPT systems based on output power  $P_o$ , separation distances between capacitive plates  $d$ , system's efficiency  $\eta$ , operating frequency  $f$ , power converter applied, and application of the system. By comparing to the past CPT system that utilized Class-E topology [11], [12], [23], [24], the proposed CPT system was able to achieve high efficiency of 88.04% in simulation and 84.60% in experiment while maintaining the ZVS condition and equip with wider load range,  $50 \Omega < R_L < 1,316 \Omega$ . Besides, this paper proves that the selected double-sided LC matching circuit could help to reduce the sensitivity of CPT system towards load and coupling variation.

Table 3. Comparison of past research for low-power CPT system

Reference	$P_o$ (W)	$d$ (mm)	$\eta$ (%)	$f$ (Hz)	Power Converter	Plate Structure	Application	Remark
[8]	12	0.07	50	6.78M	Full-bridge	Four-plate	Drone	CPT system has low efficiency and low transfer distance
[9]	8	-	77	60k	Full-bridge	Four-plate	Drone (UAV)	Full-bridge inverter needs complicated drivers
[19]	10	-	94	8k	Full-bridge	-	-	CPT system achieved high efficiency but the full-bridge inverter needs a complicated driver
[20]	10	-	70	1M	Half-bridge	Four-plate	-	CPT system has low efficiency and the half-bridge inverter needs a complicated driver
[10]	5	2	22.5	1.45M	Current-fed push-pull resonant inverter	Two-plate	Variable message sign	CPT system has very low efficiency
[23]	0.83	-	98.6	13.56M	Class-E ( $\pi$ 1a Matching)	-	-	CPT system achieved high efficiency but was sensitive to load variation
[21]	5	-	65	1M	Half-bridge	Four-plate	-	CPT system has low efficiency
[11]	5.5	0.1	83.33	1M	Class-E	Two-plate	Rotary	CPT system achieved high efficiency but the transfer distance is very short
[12]	20	5	80	6.78M	Class-E	Four-plate	Rotary	CPT system achieved high efficiency but was sensitive to load variation
[24]	2	5	74.1	1M	Class-E	Four-plate	-	CPT system has low efficiency
[13]	6	-	80	500k	Full-bridge	Four-plate	Dynamic load charging	Full-bridge inverter needs complicated drivers
This work	10	1	84.6	1M	Class-E (LCCL Matching)	Four-plate	-	CPT system has high efficiency and a wider load range

## 4. CONCLUSION

Nowadays, CPT is becoming an increasingly popular technology for delivering electrical energy, enabling higher mobility, convenience, and safety throughout whole industrial and consumer applications. As a result, this paper mainly focuses on CPT which could achieve ZVS condition and provide output power,  $P_o = 8.02$  W and efficiency,  $\eta=84.6\%$  within a small gap distance,  $d = 1$  mm. This output power is sufficient for low-power charging applications in USB interface, LED driving, and charging handheld devices such as mobile phones, laptops, and tablets. By applying a double-sided LC compensation circuit, this CPT system is less sensitive to load and gap distance variations. Besides, it makes the load range wider, which is from  $50 \Omega$  to  $1,316 \Omega$  while maintaining its ZVS conditions. In the future, it is advisable to replace the full-wave rectifier with a Class-E rectifier which can achieve 100% efficiency theoretically in the rectifier part, in turn improving the overall system's efficiency.

## ACKNOWLEDGEMENTS

This study is funded by the Ministry of Higher Education (MOHE) of Malaysia through the Fundamental Research Grant Scheme (FRGS), No: FRGS/1/2021/TK0/UTEM/02/14. The Authors also would like to thank Universiti Teknikal Malaysia Melaka (UTeM) for all the support.

## REFERENCES




- [1] C. Liu and A. P. Hu, "Steady state analysis of a capacitively coupled contactless power transfer system," in *2009 IEEE Energy Conversion Congress and Exposition*, 2009, pp. 3233–3238, doi: 10.1109/ECCE.2009.5316216.
- [2] M. Kline, I. Izyumin, B. Boser, and S. Sanders, "Capacitive power transfer for contactless charging," in *Conference Proceedings -*

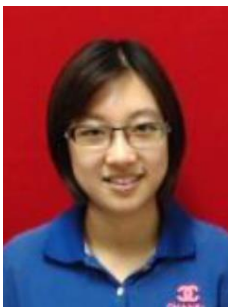
- IEEE Applied Power Electronics Conference and Exposition - APEC*, 2011, pp. 1398–1404, doi: 10.1109/APEC.2011.5744775.
- [3] J. Dai and D. C. Ludois, "A survey of wireless power transfer and a critical comparison of inductive and capacitive coupling for small gap applications," *IEEE Transactions on Power Electronics*, vol. 30, no. 11, pp. 6017–6029, 2015, doi: 10.1109/TPEL.2015.2415253.
- [4] C.-H. Lin *et al.*, "Comprehensive analysis of IPT v/s CPT for wireless EV charging and effect of capacitor plate shape and foreign particle on CPT," *Processes*, vol. 9, no. 9, Sep. 2021, doi: 10.3390/pr9091619.
- [5] Y. Wang, H. Zhang, and F. Lu, "Review, analysis, and design of four basic CPT topologies and the application of high-order compensation networks," *IEEE Transactions on Power Electronics*, vol. 37, no. 5, pp. 6181–6193, 2022, doi: 10.1109/TPEL.2021.3131625.
- [6] K. K. Hasan, S. Saat, Y. Yusop, H. Husin, and N. D. M. Sin, "The design of an efficient class E-LCCL capacitive power transfer system through frequency tuning method," *International Journal of Electrical and Computer Engineering (IJECE)*, vol. 11, no. 2, pp. 1095–1104, 2021, doi: 10.11591/ijece.v11i2.pp1095-1104.
- [7] F. Lu, H. Zhang, and C. Mi, "A review on the recent development of capacitive wireless power transfer technology," *Energies*, vol. 10, no. 11, 2017, doi: 10.3390/en10111752.
- [8] T. M. Mostafa, A. Muharam, and R. Hattori, "Wireless battery charging system for drones via capacitive power transfer," *2017 IEEE PELS Workshop on Emerging Technologies: Wireless Power Transfer, WoW 2017*, pp. 4–9, 2017, doi: 10.1109/WoW.2017.7959357.
- [9] A. Muharam, T. M. Mostafa, and R. Hattori, "Design of power receiving side in wireless charging system for UAV application," in *2017 International Conference on Sustainable Energy Engineering and Application (ICSEEA)*, Oct. 2017, pp. 133–139, doi: 10.1109/ICSEEA.2017.8267698.
- [10] L. J. Zou and A. P. Hu, "A contactless single-wire CPT (capacitive power transfer) power supply for driving a variable message sign," *2018 IEEE PELS Workshop on Emerging Technologies: Wireless Power Transfer (WoW)*, Montreal, QC, Canada, 2018, pp. 1–5, doi: 10.1109/WoW.2018.8450894.
- [11] N. Nabila, S. Saat, Y. Yusop, M. S. M. Isa, and A. A. Basari, "The design of auto-tuning capacitive power transfer for rotary applications using phased-locked-loop," *International Journal of Power Electronics and Drive Systems (IJPEDS)*, vol. 10, no. 1, pp. 307–318, 2019, doi: 10.11591/ijpeds.v10.i1.pp307-318.
- [12] S. Ahmad, A. Muharam, and R. Hattori, "Rotary capacitive power transfer with class-E inverter and balun circuit," in *2020 IEEE PELS Workshop on Emerging Technologies: Wireless Power Transfer (WoW)*, Nov. 2020, pp. 330–333, doi: 10.1109/WoW47795.2020.9291269.
- [13] G. Jing, Y. Li, Z. Zhang, C. Qian, Q. Gong, and Y. Jing, "Capacitive coupling wireless energy transmission constant voltage system based on composite network resonance," *Proceedings of the 16th IEEE Conference on Industrial Electronics and Applications, ICIEA 2021*, pp. 797–802, 2021, doi: 10.1109/ICIEA51954.2021.9516135.
- [14] A. Malsy and L. Klemm, "Distinction of gem spinels from the Himalayan mountain belt," *Chimia*, vol. 64, no. 10, pp. 741–746, 2010, doi: 10.2533/chimia.2010.741.
- [15] E. Asa, M. Mohammad, O. C. Onar, J. Pries, V. Galigekere, and G. J. Su, "Review of safety and exposure limits of electromagnetic fields (EMF) in wireless electric vehicle charging (WEVC) applications," in *2020 IEEE Transportation Electrification Conference and Expo*, 2020, pp. 17–24, doi: 10.1109/ITEC48692.2020.9161597.
- [16] T. Meade, D. O'Sullivan, R. Foley, C. Achimescu, M. Egan, and P. McCloskey, "Parasitic inductance effect on switching losses for a high frequency Dc-Dc converter," in *Conference Proceedings - IEEE Applied Power Electronics Conference and Exposition - APEC*, 2008, pp. 3–9, doi: 10.1109/APEC.2008.4522692.
- [17] W. S. Park, D. J. Thompson, and N. S. Ferguson, "Variability of the coupling loss factor between two coupled plates," *Journal of Sound and Vibration*, vol. 279, no. 3–5, pp. 557–579, 2005, doi: 10.1016/j.jsv.2003.11.035.
- [18] N. Mohammad, M. Quamruzzaman, M. R. T. Hossain, and M. R. Alam, "Parasitic effects on the performance of DC-DC SEPIC in photovoltaic maximum power point tracking applications," *Smart Grid and Renewable Energy*, vol. 04, no. 01, pp. 113–121, 2013, doi: 10.4236/sgre.2013.41014.
- [19] T. R. Amalraj, B. M. Jos, and A. M. Kottalil, "Feed forward controlled dual buck full-bridge inverter," in *Proceedings of 2017 IEEE International Conference on Technological Advancements in Power and Energy: Exploring Energy Solutions for an Intelligent Power Grid, TAP Energy 2017*, 2018, pp. 1–6, doi: 10.1109/TAPENERGY.2017.8397368.
- [20] D. Bui, T. M. Mostafa, A. P. Hu, and R. Hattori, "DC-DC converter based impedance matching for maximum power transfer of CPT system with high efficiency," 2018, doi: 10.1109/WoW.2018.8450929.
- [21] T. M. Mostafa, D. Bui, A. Muharam, R. Hattori, and A. P. Hu, "A capacitive power transfer system with a CL network for improved system performance," in *2018 IEEE Wireless Power Transfer Conference*, 2018, pp. 5–8, doi: 10.1109/WPT.2018.8639497.
- [22] A. Ayachit, F. Corti, A. Reatti, and M. K. Kazimierczuk, "Zero-voltage switching operation of transformer class-E inverter at any coupling coefficient," *IEEE Transactions on Industrial Electronics*, vol. 66, no. 3, pp. 1809–1819, 2019, doi: 10.1109/TIE.2018.2838059.
- [23] M. Meor, S. Saat, Y. Yusop, H. Husin, Z. Mustapa, and K. K. Hasan, "Design and analysis capacitive power transfer (CPT) with and without  $\pi$ 1a impedance matching circuit for 13.56MHz operating frequency," in *2018 8th IEEE International Conference on Control System, Computing and Engineering (ICCSCE)*, Nov. 2018, pp. 99–104, doi: 10.1109/ICCSCE.2018.8685020.
- [24] H. Ueda and H. Koizumi, "Class-E DC-DC converter with basic class-E inverter and class-E ZCS rectifier for capacitive power transfer," *IEEE Transactions on Circuits and Systems II: Express Briefs*, vol. 67, no. 5, pp. 941–945, 2020, doi: 10.1109/TCSII.2020.2981131.
- [25] K. Kamarudin, S. Saat, and Y. Yusmarnita, "Analysis and design of wireless power transfer: a capacitive based method," in *2014 IEEE Symposium on Industrial Electronics and Applications (ISIEA)*, Sep. 2014, pp. 136–141, doi: 10.1109/ISIEA.2014.8049886.
- [26] G. D. Singh and N. Nallam, "An RF choke-less class e power amplifier," *IEEE Transactions on Circuits and Systems II: Express Briefs*, vol. 67, no. 11, pp. 2422–2426, 2020, doi: 10.1109/TCSII.2020.2966552.
- [27] H. Zhang, F. Lu, H. Hofmann, W. Liu, and C. C. Mi, "Six-plate capacitive coupler to reduce electric field emission in large air-gap capacitive power transfer," *IEEE Transactions on Power Electronics*, vol. 33, no. 1, pp. 665–675, 2018, doi: 10.1109/TPEL.2017.2662583.
- [28] F. K. A. Rahman, S. Saat, A. Khafé, Y. Yusop, S. H. Husin, and M. H. Jamaluddin, "Efficiency comparison of capacitive wireless power transfer for different materials," *International Journal of Power Electronics and Drive Systems (IJPEDS)*, vol. 11, no. 1, pp. 200–212, 2020, doi: 10.11591/ijpeds.v11.i1.pp200-212.
- [29] W. Liu, Y. Wang, and J. Song, "Research on Schottky diode with high rectification efficiency for relatively weak energy wireless harvesting," *Superlattices and Microstructures*, vol. 150, 2021, doi: 10.1016/j.spmi.2020.106639.
- [30] F. H. Raab, "Effects of circuit variations on the class E tuned power amplifier," *IEEE Journal of Solid-State Circuits*, vol. SC-13, no. 2, pp. 239–247, 1978, doi: 10.1109/JSSC.1978.1051026.




- [31] Y. Yusop, S. Saat, H. Husin, S. K. Nguang, and I. Hindustan, "Analysis of class-E LC capacitive power transfer system," *Energy Procedia*, vol. 100, no. September, pp. 287–290, 2016, doi: 10.1016/j.egypro.2016.10.179.
- [32] Y. Yusop *et al.*, "A study of capacitive power transfer using class-e resonant inverter," *Asian Journal of Scientific Research*, vol. 9, no. 5, pp. 258–265, 2016, doi: 10.3923/ajsr.2016.258.265.
- [33] R. Larson, R. P. Hostetler, and B. H. Edwards, *Calculus: early transcendental functions*, 7th ed. Cengage Learning, Jan. 2018.
- [34] A. A. S. Mohamed, A. Berzoy, F. G. N. De Almeida, and O. Mohammed, "Modeling and assessment analysis of various compensation topologies in bidirectional IWPT system for EV applications," *IEEE Transactions on Industry Applications*, vol. 53, no. 5, pp. 4973–4984, 2017, doi: 10.1109/TIA.2017.2700281.
- [35] C. Mi, "High power capacitive power transfer for electric vehicle charging applications," in *2015 6th International Conference on Power Electronics Systems and Applications: Electric Transportation - Automotive, Vessel and Aircraft, PESA 2015*, 2016, pp. 12–15, doi: 10.1109/PESA.2015.7398937.
- [36] F. Lu, H. Zhang, and C. Mi, "A two-plate capacitive wireless power transfer system for electric vehicle charging applications," *IEEE Transactions on Power Electronics*, vol. 33, no. 2, pp. 964–969, 2018, doi: 10.1109/TPEL.2017.2735365.
- [37] M. Kasper, R. M. Burkart, G. Deboy, and J. W. Kolar, "ZVS of power MOSFETs revisited," *IEEE Transactions on Power Electronics*, vol. 31, no. 12, pp. 8063–8067, 2016, doi: 10.1109/TPEL.2016.2574998.
- [38] D. C. Marian K. Kazimierczuk, *Resonant power converters*, 2nd ed., vol. 15, no. 9. Wiley-ISTE, 1995.

## BIOGRAPHIES OF AUTHORS






**Yusmarnita Yusop**    was born in Melaka, Malaysia in 1979. She received a B.Eng in electrical engineering (mechatronic) from Universiti Teknologi Malaysia, in 2001, an M.Eng degree in electrical engineering from Kolej Universiti Tun Hussein Onn, Malaysia, in 2004, and a Ph.D. degree in electrical engineering (Capacitive power transfer) from Universiti Teknikal Malaysia Melaka in 2018. Her career as an academician began in 2005 as a teaching engineer at the Department of Industrial Electronic, Technical University Malaysia Malacca and now she is a senior lecturer at the same university. Her area of research interests includes electronic system design, wireless power transfer, and power electronics. She can be contacted at email: yusmarnita@utem.edu.my.






**Yan Qi Cheok**    was born in Muar, Malaysia in 1995. She received the B.Eng. from Universiti Malaysia Melaka, Melaka, Malaysia in 2019. She is now pursuing her master's degree in electronic engineering at Universiti Malaysia Melaka since September 2019. Her research field includes wireless power transfer systems specifically in capacitive power transfer. She can be contacted at email: m021910027@student.utem.edu.my.



**Shakir Saat**    was born in Kedah, Malaysia, in 1981. He received a B.Eng. and M.Eng. degrees in electrical engineering from the Universiti Teknologi Malaysia, Malaysia, in 2002 and 2006, respectively, and the Ph.D. degree in electrical engineering (Nonlinear control theory) from the University of Auckland, New Zealand, in 2013. He is now an associate professor and dean of the Faculty of Electronic and Computer Engineering, at Universiti Teknikal Malaysia Melaka. His research interest is in nonlinear systems control theory and wireless power transfer technologies. He has published one monograph (published by Springer Verlag) on polynomial control systems and many journals and conference papers mostly published in high-quality journals such as the International Journal of Robust and Nonlinear Control, and IET Control. He can be contacted at email: shakir@utem.edu.my.



**Huzaimah Husin**    received the B.Eng. in 2000 from Multimedia University, and M.Eng. in 2005 from Kolej Universiti Tun Hussein Onn, Malaysia respectively. She was first appointed as an engineering instructor in 2001 at Kolej Universiti Teknikal Malaysia Melaka and promoted to lecturer in 2005 and senior lecturer in 2008 in the Department of Industrial Electronics, Faculty of Electronic and Computer Engineering at Universiti Teknikal Malaysia Melaka. Since September 2014, she has been pursuing PhD in advanced control technology that focuses on acoustics energy transfer. She can be contacted at: huzaimah@utem.edu.my.